Journal Pre-proof

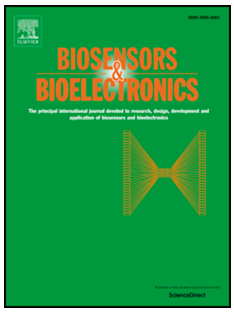

Integrated electrochemical measurement of endothelial permeability in a 3d hydrogel-based microfluidic vascular model

Jeremy F. Wong, Michael D. Mohan, Edmond W.K. Young, Craig A. Simmons

PII: S0956-5663(19)30836-X

DOI: https://doi.org/10.1016/j.bios.2019.111757

Reference: BIOS 111757

To appear in: *Biosensors and Bioelectronics*

Received Date: 30 July 2019

Revised Date: 23 September 2019

Accepted Date: 1 October 2019

Please cite this article as: Wong, J.F., Mohan, M.D., Young, E.W.K., Simmons, C.A., Integrated electrochemical measurement of endothelial permeability in a 3d hydrogel-based microfluidic vascular model, *Biosensors and Bioelectronics* (2019), doi: https://doi.org/10.1016/j.bios.2019.111757.

CRediT author statement

Jeremy Wong: conceptualization, methodology, validation, formal analysis, investigation, writing – original draft, visualization. **Michael Mohan:** methodology, writing – review & editing. **Edmond Young:** resources, writing – review & editing, supervision, funding acquisition. **Craig Simmons:** conceptualization, resources, writing – review & editing, supervision, funding acquisition

INTEGRATED ELECTROCHEMICAL MEASUREMENT OF ENDOTHELIAL PERMEABILITY IN A 3D HYDROGEL-BASED MICROFLUIDIC VASCULAR MODEL

Jeremy F. Wong[a,b], Michael D. Mohan[c], Edmond W. K. Young[a,c], Craig A. Simmons[a,b,c*]

[a] Institute of Biomaterials and Biomedical Engineering, University of Toronto, Toronto, ON M5S 3G9, Canada

[b] Translational Biology and Engineering Program, Ted Rogers Centre for Heart Research, Toronto, ON M5G 1M1, Canada

[c] Department of Mechanical & Industrial Engineering, University of Toronto, Toronto, ON M5S 3G8, Canada

[*] Corresponding author: Craig A. Simmons. E-mail: c.simmons@utoronto.ca. Telephone: 1-416-946-0548. Address: U of T Translational Biology & Engineering Program, Ted Rogers Centre for Heart Research, MaRS West Tower, 661 University Avenue, 14th Floor, Toronto, Ontario M5G 1M1 Canada.

Abstract

Mimicking the physiological or pathophysiological barrier function of endothelial and epithelial cells is an essential consideration in organ-on-a-chip models of numerous tissues including the vascular system, lungs, gut and blood-brain barrier. Recent models have furthermore incorporated 3D extracellular matrix hydrogels to recapitulate the composition and cell-matrix interactions found in the native microenvironment. Assessment of barrier function in these 3D organ-on-a-chip models, however, is typically limited to diffusive permeability measurements that are exclusively fluorescence-based. In this work, an on-chip electrochemical method to measure endothelial permeability in a 3D hydrogel-based vascular model was developed that replaces the ubiquitous fluorescent tracer with an electroactive one. Unlike the traditional fluorescent-based method, this electrochemical method eliminates the need for bulky, costly and complex optical instrumentation that require measurements to be performed outside of the incubator. A 3D extracellular matrix gel-based microfluidic model was first developed that incorporates capillary pressure barrier microstructures. Micromilling of thermoplastics was used to fabricate these microstructures in a rapid, moldless fashion. As a proof-of-concept demonstration, the permeability of endothelial cells cultured on hydrogels was electrochemically measured after being subject to perfusion conditions, and following exposure to known permeability mediators. In summary, the electrochemical permeability assay possesses both the benefits of on-chip integration and robustness of the traditional fluorescent-based assay while also enabling the measurement of barrier function in an organ-on-a-chip incorporating 3D culture conditions.

Keywords

Endothelial permeability; biosensor; microphysiological system; 3D culture; transendothelial electrical resistance

Introduction

Barrier-forming tissues are found throughout the human body in the form of epithelia and endothelia that line the intestines, lungs, blood vessels, and the vasculature of the blood-brain barrier. These tissues form selective semipermeable barriers that regulate biomolecular transport between adjacent tissues. *In vitro* cell culture models of such tissues must therefore mimic *in vivo* physiological barrier function, particularly in pharmaceutical drug discovery where drug transport is modeled (Arık et al., 2018; Sakolish et al., 2016; Yeste et al., 2018).

Barrier function is predominantly assessed *in vitro* in the well-known Transwell system where cell monolayers are cultured on a porous membrane support vertically separating two fluidic chambers. The porous membrane, however, is typically made of a stiff, artificial polymer film that differs significantly from the extracellular matrix (ECM) of the native microenvironment (Baker and Chen, 2012). Recently, microfluidic organ-on-a-chip models of barrier-forming tissues have sought to address this limitation by integrating biomimetic hydrogels that better recapitulate 3-dimensional *in vivo* cell-ECM interactions and substrate stiffness (Lee et al., 2015, 2018). Indeed, cell-ECM interactions are known to regulate barrier function and interendothelial junction integrity (del Zoppo and Milner, 2006; Minshall and Malik, 2006), stressing the need for more *in vivo*-like 3D culture models. Unlike traditional *in vitro* models, microphysiological systems also enable additional spatiotemporal control over the microenvironment *via* dynamic cell culture conditions based on the incorporation of features such as perfusion flow, biomechanical forces and biochemical gradients.

In both macroscale and microfluidic Transwell-based systems, epithelial/endothelial permeability and trans-epithelial/endothelial electrical resistance (TEER) are the two most common metrics of barrier function. Permeability is a measure of the paracellular diffusive flux of a fluorescent tracer molecule across a barrier-forming cell monolayer while TEER is a measure of paracellular ionic conductance. Both methods, however, have limitations in the context of 3D hydrogel-based microfluidic models. TEER measurements in such models remain subject to possible measurement errors due to non-uniform current densities that are strongly dependent on factors such as electrode positioning and microchannel geometry (Srinivasan et al., 2015). Barrier function assessment in 3D culture models is therefore almost exclusively performed using fluorescent tracer-based permeability assays (Polacheck et al., 2019; Trietsch et al., 2017; Zervantonakis et al., 2012) that require complex, costly and bulky fluorescence imaging instrumentation. These assays are typically limited to off-chip, low throughput, endpoint measurements.

We previously introduced an electrochemical permeability assay in a Transwell-based microfluidic model (Wong and Simmons, 2019) where the ubiquitous fluorescent tracer was replaced with an electrochemical tracer that could be detected on-chip using a set of device-integrated electrodes. Here, we extend the electrochemical permeability assay to a 3D ECM hydrogel-based microfluidic vascular model that better recapitulates the native cellular microenvironment. It enables endothelial permeability to be monitored directly on-chip inside the incubator environment, and substitutes bulky, complex and costly fluorescence instrumentation with low footprint, cost-effective electronic instrumentation. The method is therefore suitable for high throughput applications, and combines the robustness of tracer-based permeability assays with the advantages of on-chip integration. Ultimately, we demonstrate that the electrochemical permeability assay can operate in 3D organ-on-a-chip models of increasing sophistication and

physiological relevance, a more challenging environment for assay integration than traditional Transwell-based models.

Results

ECM gel–based microfluidic vascular model with integrated electrodes

A cross-sectional schematic of the ECM hydrogel-based microfluidic vascular model with integrated electrochemical sensing is shown in Figure 1a, and consists of two adjacent microchannels separated by a narrow ridge-like structure called a phaseguide, as well as a three-electrode electrochemical cell. The phaseguide, a capillary pressure barrier (Vulto et al., 2006), serves to pin and confine the hydrogel to the gel microchannel without the need for micropillars, restricting its advancement into the cell culture microchannel and leaving an open interface between the two microchannels. This produces a surface composed of a native ECM protein on which a cell monolayer may be cultured (Trietsch et al., 2017; van Duinen et al., 2017), incorporating cell-ECM interactions and a semi-lumen-like architecture that are not present in traditional Transwell-based models. Two compartments are therefore formed: the microchannel through which culture medium can flow and the ECM gel, mimicking a blood vessel lumen and the subendothelial space, respectively. The integrated electrodes are located on the bottom surface of the gel compartment and are embedded in the hydrogel. The porosity of the ECM gel allows diffusion of molecules to the electrode surface. An illustration of the device and electrochemical permeability assay is shown in Figure 1b.

The assembled device is composed of three layers: the electrode, fluidic and media reservoir layers (Figure 1c). The thin-film gold electrodes were patterned onto a glass substrate while the microchannels were fabricated out of poly(methyl methacrylate) (PMMA), a transparent thermoplastic. Despite the utility of polydimethylsiloxane (PDMS) in the prototyping of microfluidic devices, thermoplastics are more suitable for eventual high-volume production with the availability of methods such as hot embossing and injection molding (Berthier et al., 2012; Halldorsson et al., 2015). Moreover, PDMS is known to absorb small hydrophobic molecules, which may adversely impact cell culture, assay readouts, and pharmaceutical drug discovery studies (Moore et al., 2017). Although a glass electrode substrate was used here, methods to pattern electrodes on thermoplastic substrates exist (Gharib Naseri et al., 2008; Liu et al., 2013), leaving the possibility for an all-thermoplastic device. Figure 1d shows an image of the assembled microfluidic chip where each chip consisted of two sensor-integrated microfluidic devices. A magnified image of the integrated gold electrodes in the gel microchannel is also shown. The phaseguide is visible as the narrow rectangular structure between the microchannels. Each device occupied approximately the area of a single well in a 48-well plate, a footprint that is readily arrayable for higher throughput implementations of the device and assay.

The principle of the electrochemical permeability assay is illustrated in Figure 1e where a concentrated electroactive tracer solution is first injected at a fixed flow rate into the cell culture channel inlet. The ensuing concentration gradient between cell culture and gel microchannels results in the diffusion of the electroactive tracer across the endothelial cell monolayer into the ECM hydrogel due the porous nature of the gel (Ramanujan et al., 2002), mimicking physiological diffusion of biomolecules in the subendothelial tissue space. The peak voltammetric current measured at the gel-embedded electrodes is proportional to the concentration of electroactive tracer, enabling the rate of accumulation in tracer concentration to be

continuously monitored and used to calculate the endothelial permeability. A sample set of square wave voltammetry curves acquired while performing the electrochemical permeability assay is shown in Figure S1. A lower rate of tracer diffusive transport corresponds to a lower endothelial permeability, which is indicative of well-formed intercellular junctions and greater barrier function. Relative to standard fluorescence-based permeability assays, the use of integrated electrodes eliminates the need for complex and costly optical instrumentation and allows endothelial permeability measurements to be rapidly performed directly on-chip inside the incubator environment.

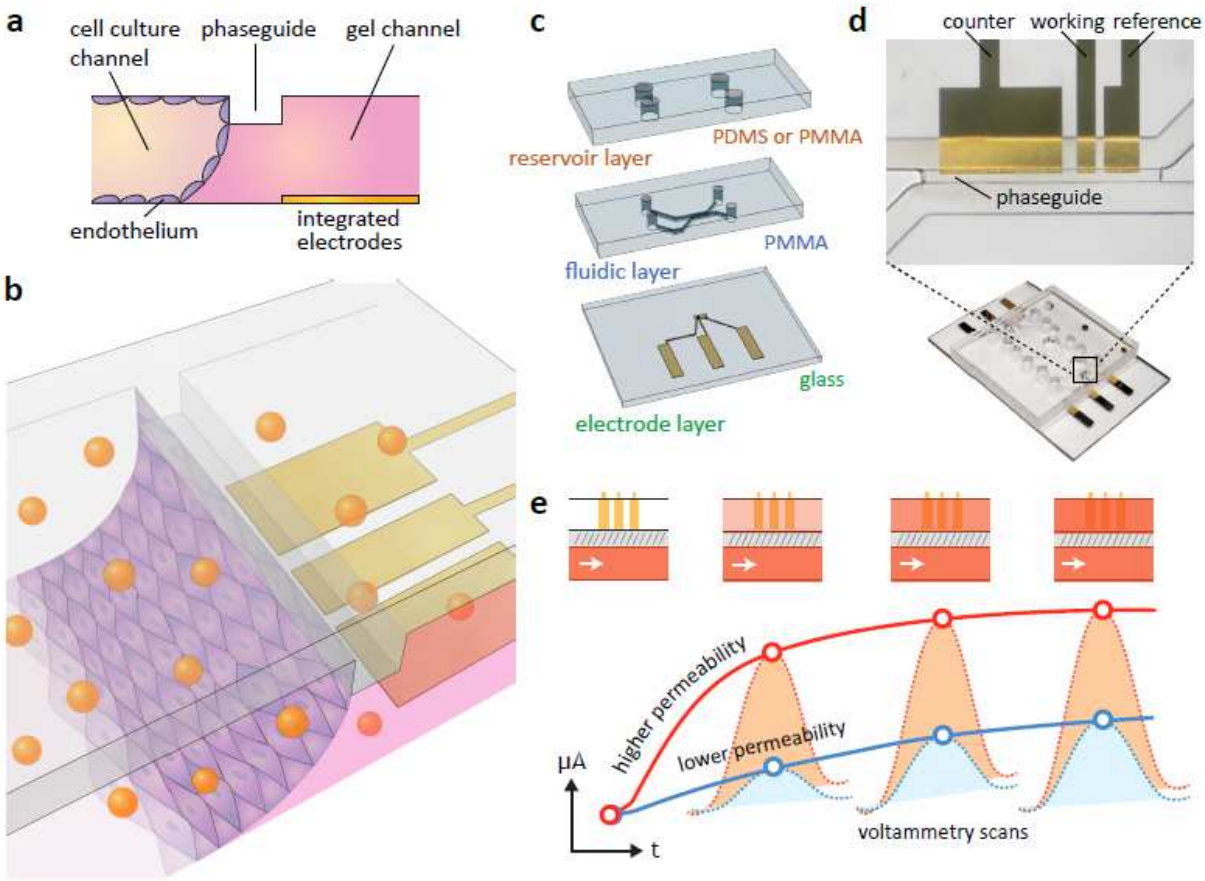

Figure 1 a) Cross-sectional view, **b)** 3D illustration and **c)** exploded view of the microdevice. The phaseguide acts as a capillary pressure barrier that confines a hydrogel to the gel channel. Cells are cultured on the curved gel surface. Gel-embedded electrodes are used to monitor diffusive transport of an electroactive tracer across the cell monolayer. **d)** Image of the assembled device, and top-down view of the phaseguide region with integrated counter, working and reference electrodes. **e)** Schematic of electrochemical permeability assay measurements. Square wave voltammetry peak currents are proportional to tracer concentrations in the gel channel. The rate of tracer accumulation in the gel channel is used to determine the endothelial permeability.

Cell culture on ECM gels pinned using micromilled phaseguides

The device microchannels and phaseguides were fabricated by direct micromilling of PMMA stock material (Figure 2a). The endmill diameter determined the microchannel width while the endmill

plunging depth into the stock material determined the microchannel height. Microchannels with a nominal height and width of 175 μm and 254 μm, respectively, were produced using this method. Phaseguides were likewise fabricated except with a smaller plunging depth to leave a ridge-like structure between the microchannels. For optimal results, it was necessary to mill the phaseguides prior to the microchannels to avoid damage. Previous methods used to fabricate phaseguide structures include photolithographic processing of a dry film photoresist (Vulto et al., 2005), injection molding of cyclic olefin-copolymer (COC) using an aluminum mold (Garbarino et al., 2016) and soft lithographic processing of PDMS with an etched silicon master (Tung et al., 2013). Unlike the aforementioned methods, direct micromilling enables the rapid and simple fabrication of different microchannel and phaseguide geometries without requiring either a mold or mask, which is advantageous in device prototyping (Guckenberger et al., 2015). A bottom-up view of the device microchannels and phaseguide is shown in Figure 2b. The circular trochoidal marks that are characteristic of milling operations are clearly visible on the microchannel surfaces. The milled PMMA phaseguide surfaces also displayed roughness that would not be present using other fabrication methods, but could be smoothed if necessary using solvent vapor polishing (Yen et al., 2016).

To determine whether or not the surface roughness compromised phaseguide function, a wide range of phaseguide dimensions were milled, and hydrogel pinning by the phaseguides was assessed. Cross-sectional images of microdevices with different phaseguide dimensions are shown in Figure 2c. A bottom-up view is shown in Figure 2d. Hydrogels were stained fluorescently and imaged using confocal microscopy in order to visualize both hydrogel and phaseguide shapes. Successful gel pinning was achieved with phaseguide heights ranging from 20-60 μm and a 110 μm width, as well as with a ~45 μm height and 15-100 μm widths. The additional surface roughness due to the milling process therefore did not prevent the phaseguides from pinning hydrogel solutions and confining them to the gel channel. Indeed, small phaseguide heights or widths were sufficient to pin the hydrogel, enabling cell-to-gel channel interfaces that spanned almost the entire microchannel height (~90%) with gel lengths on the order of millimetres. This is a significant improvement over the micropillar approach to pinning gels where lengths are typically limited to a few hundred microns. Furthermore, the slight hydrophilicity of PMMA phaseguides obviates the need for the pre-treatment steps necessary to pin gels with hydrophobic PDMS phaseguides. Phaseguides with nominal dimensions of 45 (H) × 100 (W) μm were used in all subsequent cell culture and endothelial permeability experiments, a balance between gel pinning reliability, ease of micromilling and large hydrogel surface area for culturing the endothelia.

Confinement of human umbilical vein endothelial cells (HUVECs) to the cell culture channel is shown in Figure 2e. A representative 3D volume rendering of a HUVEC monolayer in the microdevice is shown in Figure 2f. HUVECs were cultured for 72 h under bidirectional perfusion conditions on a rocker platform (Figure S2). Figure 2f confirms that the cells attached to the curved gel surface, completely covering the vertical portion of the gel up to the phaseguide. Importantly, cell invasion into the gel was not observed. Cell monolayer confluency was further evaluated by staining for VE-cadherin, an essential constituent of endothelial junctions (Vestweber, 2008). Over the entire gel surface, VE-cadherin expression was localized at the intercellular junctions along the cell periphery, which demonstrated that the monolayer was indeed confluent with well-formed junctions.

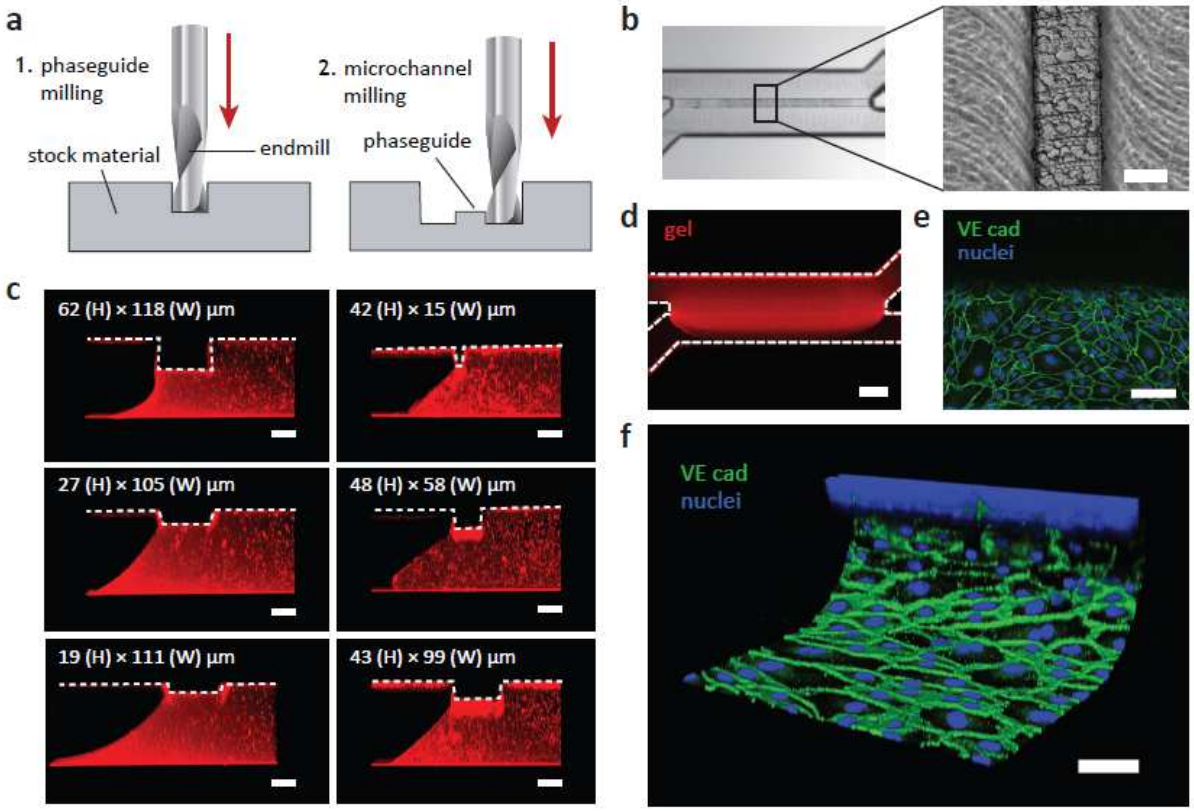

Figure 2 a) Cross-sectional schematic of phaseguide and microchannel milling. **b)** Phase contrast image of micromilled phaseguide and microchannels. Scale bar = 50 µm. **c)** Examples of collagen gel pinning (red) using micromilled phaseguides (dotted lines). Scale bars = 50 µm. **d)** Bottom-up view of pinned collagen gel in microdevice (dotted lines). Scale bar = 250 µm. **e)** Bottom-up view of HUVEC monolayer cultured for 72 h in the device. Scale bar = 100 µm. **f)** Volume rendering of HUVEC monolayer demonstrating cell attachment on vertical gel surface and intercellular junction formation. Scale bar = 50 µm. HUVECs were stained for VE-cadherin (green) and nuclei (blue).

Electrochemical permeability assay in 3D vascular model

The calculation of endothelial permeability assumes that transport of the tracer into the gel is diffusion-dominated with negligible convective transport. It was therefore necessary to select an electroactive tracer solution flow rate that satisfied this condition. A computational model of fluid flow and mass transport was used to numerically simulate the time-dependent transport of the electroactive tracer in the microdevice cell and gel channels (Figure 3a). The model, based on our previous work (Wong et al., 2017b, 2017a), was used to confirm that diffusive transport was dominant over convective transport across a wide range of conditions, including cell-free and cell-laden gels (Figure S3, Figure S4). Injection of a fluorescent tracer into the microdevice was used to experimentally visualize tracer distribution over time in the cell culture channel and collagen gel at different flow rates. Using this method, an injection flow rate of 0.180 ml h^{-1} was selected for the permeability assay, which provided a balance between rapid injection into the cell culture channel, minimal flow-induced shear stress on endothelium, and lower reagent consumption. Images of fluorescent tracer distribution over time in the device at this flow rate are shown in Figure 3b.

The electrochemical permeability assay in the 3D vascular model requires that the integrated electrodes perform measurements while embedded in the ECM gel, which could hinder electroactive tracer detection. However, in the presence of a concentrated tracer solution, the voltammetric current measured by gel-embedded electrodes was not significantly attenuated by a 2.5 mg ml^{-1} collagen gel relative to non-embedded electrodes (Figure 3c). This is an indication that the gel did not significantly decrease the electrode surface area accessible to the tracer, likely due to the small size of the tracer compared to the pores of the gel. The voltammetric current response to increasing tracer concentrations was further verified to be linear in the gel (Figure S5). The electroactive tracer could therefore be monitored using ECM gel-embedded electrodes.

The electrochemical permeability assay was performed by injecting a concentrated electroactive tracer solution into the cell culture channel at a constant flow rate, and monitoring the concentration of tracer in the gel over time using square wave voltammetry (SWV). From the measured rate of tracer accumulation, the diffusive permeability was then calculated. Hexaaminеruthenium (RuHex) was shown in our previous work to be the most suitable electroactive tracer for the permeability assay as it does not alter endothelial permeability and cell viability (Wong and Simmons, 2019). Figure 3d shows the normalized gel channel tracer concentrations over time for four experimental conditions: cell-free gels, untreated endothelial cells, EGTA-treated endothelial cells, and thrombin-treated endothelial cells. The corresponding normalized rates of diffusive tracer transport dC_{gel}/dt are shown in Figure 3e. Despite a 72 h exposure to culture medium, the electrodes produced well-defined SWV curves, and therefore have the potential to be used over longer culture periods. The apparent permeability values for each experimental condition are shown in Figure 3f. As expected, the diffusive permeability for cell-free collagen gels was the highest ($1.69\pm0.24\times10^{-4}$ cm s^{-1}), as there were no cells to slow tracer diffusion, while the endothelial permeability of untreated confluent HUVEC monolayers was the lowest ($4.62\pm0.75\times10^{-5}$ cm s^{-1}), corresponding to a well-formed endothelial barrier with tight intercellular junctions. EGTA increases endothelial permeability by chelating Ca^{2+} ions necessary for adherens junction formation (Baetscher and Brune, 1983; Lakshmikanthan et al., 2018); thrombin does the same by inducing a cellular contractile response (Rabiet et al., 1996). This was corroborated by the electrochemically measured permeabilities for EGTA- and thrombin-treated ECs ($1.27\pm0.37\times10^{-4}$ cm s^{-1} and $1.06\pm0.15\times10^{-4}$ cm s^{-1}, respectively), which were in between the values for untreated ECs and cell-free gels. Statistically significant differences in permeability were found between all groups ($p < 0.05$) with the exception of 1) gel-only and EGTA-treated HUVEC conditions ($p > 0.2$) and 2) EGTA-treated and thrombin-treated HUVEC conditions ($p > 0.65$).

A direct comparison is not possible with our previous work (Wong and Simmons, 2019) where the electrochemical permeability assay was implemented in a Transwell-based microfluidic device. However, untreated PAECs and HUVECs had similar apparent permeabilities of 3.46×10^{-5} and 4.62×10^{-5} cm s^{-1}, respectively, which indicates comparable barrier function despite the differences in endothelial cell type, culture conditions, culture substrate and device geometry. While the effect of the collagen gel on endothelial permeability was not determined in this work, it is nevertheless well-established that interactions between endothelial cells and the subendothelial matrix are important in the regulation of junction integrity and barrier function (del Zoppo and Milner, 2006; Minshall and Malik, 2006). The incorporation of a 3D ECM and cell-matrix interactions also remains critical in the development of organotypic culture models (Huh et al., 2011; Lee et al., 2018), and enables the future addition of gel-embedded stromal cells to even better mimic blood vessel architecture or tumor cells to model cancer

metastasis. Furthermore, the permeability values reported here are comparable to permeability values of $1.2\text{-}3.5\times10^{-5}$ cm s^{-1} (Bertulli et al., 2018; Ho et al., 2017) obtained using the conventional fluorescence-based permeability assay in microfluidic vascular models incorporating collagen gels with HUVEC monolayers. This was expected since the principle of both assays is identical, but differs in the tracer used and detection modality.

Currently, the on-chip assessment of endothelial barrier function in microfluidic systems is performed using impedance-based measurements (Cacopardo et al., 2019; van der Helm et al., 2016). These microfluidic systems are based on commercial platforms like ECIS and xCELLigence that perform impedance-based measurements of barrier function in standard multiwell (e.g., 96-well) culture formats. Impedance measurements enable the label-free, sensitive, rapid and high throughput measurement of barrier function. The high fluidic resistances of microfluidic channels significantly complicate integration, however, as measurements are sensitive to electrode positioning and microchannel geometry among other factors (Srinivasan et al., 2015).

It is improbable that diffusive permeability assays will possess the speed and sensitivity of commercial impedance-based systems. However, the electrochemical permeability assay has a number of advantages over traditional fluorescence-based permeability assays, namely, its on-chip integration, potential for high throughput measurements and elimination of optical instrumentation – advantages that are drawn from impedance-based techniques. The electrochemical permeability assay therefore seeks to combine the robustness of traditional permeability assays with the advantages of integrated impedance techniques. Moreover, an important consideration in impedance-based barrier function measurements in 3D microfluidic culture models is that a uniform current density across the cell monolayer is necessary for accurate impedance measurements (Srinivasan et al., 2015). This is a non-trivial challenge since cell monolayers are frequently cultured on a vertical curved surface in 3D microfluidic models instead of the horizontal planar surfaces common to standard models like Transwell or multiwell formats. Endothelial permeability and TEER measurements nonetheless remain complementary metrics of barrier function (Bischoff et al., 2016) and are both measured when possible to characterize endothelial monolayers.

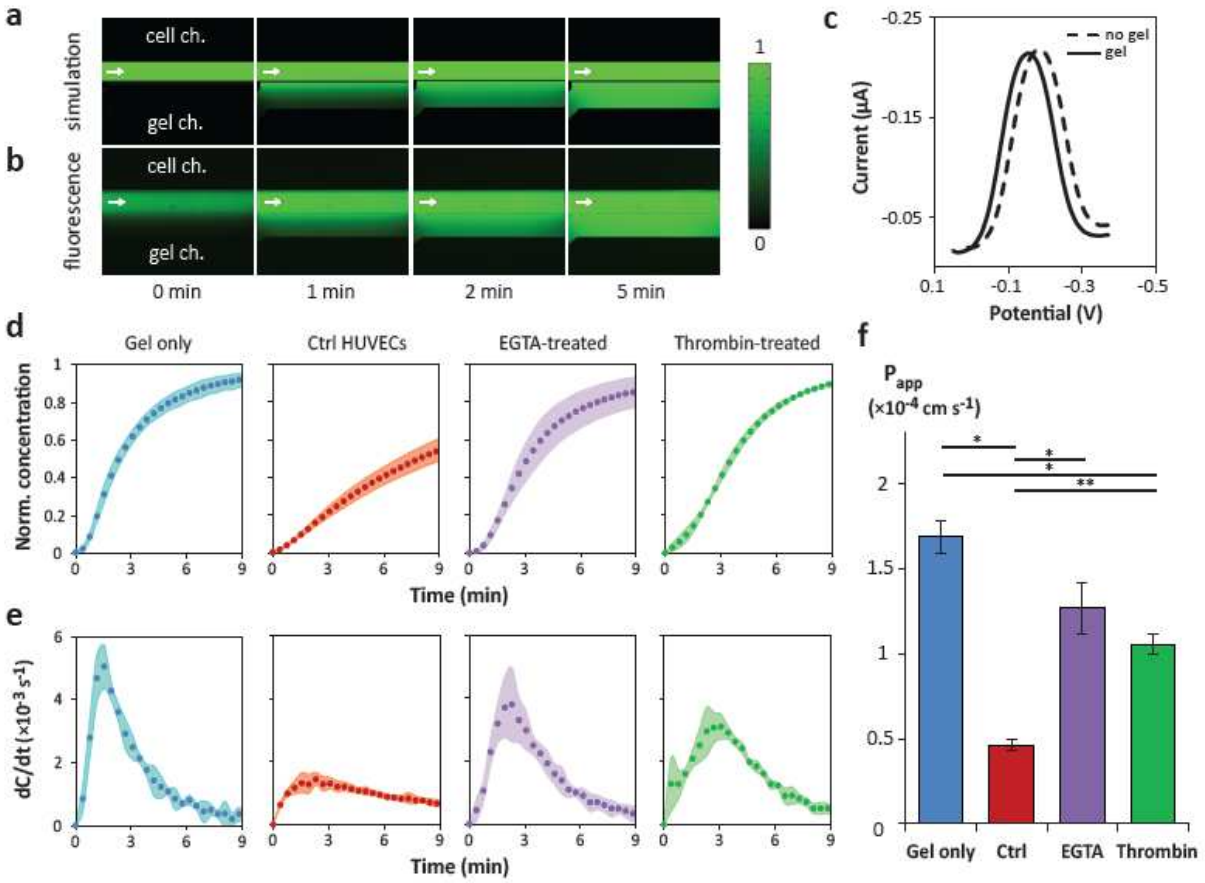

Figure 3 a) Numerically simulated visualization of tracer concentration over time in the gel channel (inlet flow velocity: 0.001 mm s^{-1}, representing an inlet flow rate of 0.180 ml h^{-1}). **b)** Experimental visualization of tracer concentration over time in the gel channel using fluorescent tracer (inlet flow rate: 0.180 ml h^{-1}). **c)** Comparison of SWV scans obtained using gel-embedded (2.5 mg ml^{-1}) and non-embedded electrodes. Electrochemical measurements of **d)** normalized concentrations and **e)** corresponding slopes over time for four experimental conditions: 2.5 mg ml^{-1} collagen gel only (n = 6); untreated control (n = 5), 4 mM EGTA-treated (n = 5) and 5 U ml^{-1} thrombin-treated HUVECs (n = 3). Shaded areas represent the standard deviation. **f)** Endothelial permeabilities measured using the on-chip electrochemical permeability assay. * $p < 0.025$, ** $p < 0.05$. Error bars represent the standard error of the mean.

Conclusion

In summary, we developed an integrated electrochemical method for measuring endothelial barrier function in a 3D ECM gel-based vascular model. The vascular model used micromilled phaseguides to confine collagen gels to the gel channel where a wide range of phaseguide dimensions were found to successfully achieve this confinement. Micromilling enabled the rapid moldless fabrication of the phaseguides. Current methods to measure endothelial permeability in 3D microenvironments are exclusively fluorescence-based. Unlike these methods, the electrochemical permeability assay enabled the measurements to be performed directly on-chip inside the incubator environment without the need for complex, expensive and bulky optical instrumentation. Moreover, due to its charge-based readout, the

assay may be readily parallelized for higher throughput measurements. Ultimately, we demonstrate the capability of the electrochemical permeability assay to measure barrier function in organs-on-chips of increasing complexity and physiological relevance while also retaining many of the benefits of lab-on-a-chip integration.

Methods

Microfluidic device fabrication

The microfluidic device consisted of three layers: 1) the substrate with patterned electrodes, 2) the fluidic layer, and 3) the media reservoir layer. The fluidic layer was fabricated by the milling of cast PMMA sheets (McMaster-Carr Supply, IL), a method useful for prototyping thermoplastic microfluidic devices (Guckenberger et al., 2015). Briefly, the microfluidic channels and phaseguides were designed in Fusion 360 (Autodesk, CA), which also enabled setting of the milling toolpaths and generation of the G-code. A PCNC770 mill (Tormach, WI) was then used to remove stock material corresponding to the microdevice features. Device geometries were machined using uncoated, 4-flute, carbide endmills of diameters 0.010", 0.015", 3/64" and 1/8" (Caliber Industrial Supply, CAN) at a common spindle speed of 5000 RPM and respective feed rates of 20, 50, 67 and 300 mm/min. Spindle speeds and feed rates were selected based on common machining practices in order to minimize machining time while also optimizing optical transparency and feature fidelity.

Media reservoir layers were fabricated by milling through-holes in PMMA sheet stock and then bonded to microchannel layers using thermal solvent-assisted bonding: 95% ethanol was injected between the two layers, which were then pressed together using a hydraulic press (Carver, IN) at 70°C for 90 s under 1000 lbf of pressure. Alternatively, media reservoir layers were fabricated by punching holes into PDMS substrates, and attached to the fluidic layers using a double-sided adhesive (Adhesives Research, PA).

For thin film electrode fabrication, soda lime glass slides coated with photoresist, Cr and Au (Telic Company, CA) were patterned using standard photolithography. Briefly, the electrode geometry was patterned onto the substrate via UV light exposure of the photoresist through a chromium photomask (μPG 501, Heidelburg Instruments, DEU). Following photoresist development, wet etching was used to selectively remove Au (TFA, Transene, MA) and Cr (CR-16, KMG Chemicals, TX). The remaining photoresist was then removed using photoresist stripper (AZ 300T, AZ Electronic Materials, NJ) and piranha treatment (3:1 H_2SO_4:H_2O_2). Finally, PMMA and glass layers were bonded together using a light curable medical device adhesive (Dymax, CT).

Microdevices were prepared for cell culture by rinsing copiously with 70% ethanol to sterilize the microchannels followed by distilled H_2O. Devices were further sterilized under UV light for at least 2 h and left to dry overnight prior to ECM hydrogel injection.

Electrochemical permeability assay

Electrochemical measurements were performed with a potentiostat (Emstat, PalmSens, NLD). Square wave voltammetry (SWV) was used to monitor electroactive tracer concentrations. The following

parameters were used to ensure a large signal and rapid scanning: 100 Hz frequency, 75 mV amplitude, 0.05 to -0.35 V scan range and an 8 mV potential step.

The electrochemical permeability assay was performed inside an incubator. Hexaammineruthenium chloride (Sigma-Aldrich, MO), the electroactive tracer, was injected at 0.180 ml h^{-1} into the cell culture channel inlet using a syringe pump (Cole-Parmer, IL). SWV scans were acquired at 20 s intervals over the duration of the assay. Measured peak currents were normalized to minimize device-to-device variations in electrode areas. The electrochemical permeability assay was considered complete when the peak currents had stabilized in value, i.e., < 1% variation was measured over 6 scan intervals, indicating that the diffusion of the tracer into the gel channel had largely ceased.

The diffusive permeability was measured for cell-free collagen gels, untreated control HUVEC monolayers, EGTA-treated HUVEC monolayers and thrombin-treated HUVEC monolayers. In all four conditions, devices were kept in the incubator for 72 h prior to measurements. EGTA treatment consisted of exposing HUVECs to 4 mM EGTA (Sigma-Aldrich, MO) in PBS for 15 min. Similarly, thrombin treatment consisted of exposing HUVECs to 5 U ml^{-1} human thrombin (Sigma-Aldrich, MO) in basal VascuLife media for 15 min following a 1h pre-treatment in basal VascuLife media supplemented with 1% FBS.

Endothelial permeability calculation

For a given tracer molecule, the apparent endothelial permeability P_{app} is calculated using the following equation (Yuan and Rigor, 2011):

$$P_{app} = \frac{1}{C_{max}} \frac{dC_{gel}}{dt} \frac{V_{gel}}{A_{gel}} \quad \text{Eq.1}$$

where C_{gel} and C_{max} are the gel channel and injected tracer solution concentrations, respectively, A_{gel} is the vertical projected area of the pinned collagen gel, and V_{gel} is the volume of the gel channel. Equation 1 assumes that the concentration in the cell channel remains at C_{max} over the duration of the permeability measurement. For the 3D gel-based vascular model, $V_{gel} = 1.25\times10^{-1}$ mm^3, and $A_{gel} = 3.81\times10^{-3}$ cm^2. C_{gel} and C_{max} were obtained from electrochemical SWV scans where the SWV peak currents were proportional to the electroactive tracer concentration. Endothelial permeability was calculated using the maximum slope measured in each device replicate.

Supporting information

Additional methods are described in the supporting information.

ACKNOWLEDGEMENTS

The authors acknowledge the financial support from Natural Sciences and Engineering Research Council of Canada (NSERC) Discovery Grant RGPIN-2016-06026 to CAS, NSERC Discovery Grant RGPIN-2019-5885 to EY. JW acknowledges the financial support from the NSERC CREATE Training Program in Organ-on-a-Chip Engineering and Entrepreneurship (TOeP), the NSERC CREATE Microfluidic Applications and Training in Cardiovascular Health (MATCH) program, and the Queen Elizabeth II

Graduate Scholarships in Science & Technology (QE-GSST) program. MM acknowledges the financial support from the Ontario Graduate Scholarship and QE-GSST programs.

REFERENCES

Arık, Y.B., van der Helm, M.W., Odijk, M., Segerink, L.I., Passier, R., van den Berg, A., van der Meer, A.D., 2018. Barriers-on-chips: Measurement of barrier function of tissues in organs-on-chips. Biomicrofluidics 12, 042218. https://doi.org/10.1063/1.5023041

Baetscher, M., Brune, K., 1983. An in vitro system for measuring endothelial permeability under hydrostatic pressure. Exp. Cell Res. 148, 541–547. https://doi.org/10.1016/0014-4827(83)90178-7

Baker, B.M., Chen, C.S., 2012. Deconstructing the third dimension – how 3D culture microenvironments alter cellular cues. J. Cell Sci. 125, 3015–3024. https://doi.org/10.1242/jcs.079509

Berthier, E., Young, E.W.K., Beebe, D., 2012. Engineers are from PDMS-land, biologists are from polystyrenia. Lab Chip 12, 1224–1237. https://doi.org/10.1039/c2lc20982a

Bertulli, C., Gerigk, M., Piano, N., Liu, Y., Zhang, D., Müller, T., Knowles, T.J., Huang, Y.Y.S., 2018. Image-Assisted Microvessel-on-a-Chip Platform for Studying Cancer Cell Transendothelial Migration Dynamics. Sci. Rep. 8, 12480. https://doi.org/10.1038/s41598-018-30776-0

Bischoff, I., Hornburger, M.C., Mayer, B.A., Beyerle, A., Wegener, J., Fürst, R., 2016. Pitfalls in assessing microvascular endothelial barrier function: impedance-based devices versus the classic macromolecular tracer assay. Sci. Rep. 6, 23671. https://doi.org/10.1038/srep23671

Cacopardo, L., Costa, J., Giusti, S., Buoncompagni, L., Meucci, S., Corti, A., Mattei, G., Ahluwalia, A., 2019. Real-time cellular impedance monitoring and imaging of biological barriers in a dual-flow membrane bioreactor. Biosens. Bioelectron. 140, 111340. https://doi.org/10.1016/j.bios.2019.111340

del Zoppo, G.J., Milner, R., 2006. Integrin–Matrix Interactions in the Cerebral Microvasculature. Arterioscler. Thromb. Vasc. Biol. 26, 1966–1975. https://doi.org/10.1161/01.ATV.0000232525.65682.a2

Garbarino, F., Kistrup, K., Rizzi, G., Hansen, M.F., 2016. Burst pressure of all-polymer phaseguide structures of different heights. 20th Int. Conf. Miniaturized Syst. Chem. Life Sci. MicroTAS 2016.

Gharib Naseri, N., Baldock, S.J., Economou, A., Goddard, N.J., Fielden, P.R., 2008. Disposable injection-moulded cell-on-a-chip microfluidic devices with integrated conducting polymer electrodes for on-line voltammetric and electrochemiluminescence detection. Electroanalysis 20, 448–454. https://doi.org/10.1002/elan.200704074

Guckenberger, D.J., De Groot, T.E., Wan, A.M.D., Beebe, D.J., Young, E.W.K., 2015. Micromilling: A method for ultra-rapid prototyping of plastic microfluidic devices. Lab Chip 15, 2364–2378. https://doi.org/10.1039/c5lc00234f

Halldorsson, S., Lucumi, E., Gómez-Sjöberg, R., Fleming, R.M.T., 2015. Advantages and challenges of microfluidic cell culture in polydimethylsiloxane devices. Biosens. Bioelectron. 63, 218–231. https://doi.org/10.1016/j.bios.2014.07.029

Ho, Y.T., Adriani, G., Beyer, S., Nhan, P.-T., Kamm, R.D., Kah, J.C.Y., 2017. A Facile Method to Probe

the Vascular Permeability of Nanoparticles in Nanomedicine Applications. Sci. Rep. 7, 707. https://doi.org/10.1038/s41598-017-00750-3

Huh, D., Hamilton, G.A., Ingber, D.E., 2011. From 3D cell culture to organs-on-chips. Trends Cell Biol. 21, 745–754. https://doi.org/10.1016/j.tcb.2011.09.005

Lakshmikanthan, S., Sobczak, M., Li Calzi, S., Shaw, L., Grant, M.B., Chrzanowska-Wodnicka, M., 2018. Rap1B promotes VEGF-induced endothelial permeability and is required for dynamic regulation of the endothelial barrier. J. Cell Sci. 131, jcs207605. https://doi.org/10.1242/jcs.207605

Lee, D.-H., Bae, C.Y., Kwon, S., Park, J.-K., 2015. User-friendly 3D bioassays with cell-containing hydrogel modules: narrowing the gap between microfluidic bioassays and clinical end-users' needs. Lab Chip 15, 2379–87. https://doi.org/10.1039/c5lc00239g

Lee, S., Ko, J., Park, D., Lee, S.-R., Chung, M., Lee, Y., Jeon, N.L., 2018. Microfluidic-based vascularized microphysiological systems. Lab Chip 18, 2686–2709. https://doi.org/10.1039/C8LC00285A

Liu, J., Qin, J., Li, J., Li, D., Xu, Z., Zhang, X., Du, L., Liu, C., 2013. Monolithic integration of three-material microelectrodes for electrochemical detection on PMMA substrates. Electrochem. commun. 31, 20–23. https://doi.org/10.1016/j.elecom.2013.02.024

Minshall, R.D., Malik, A.B., 2006. Transport Across the Endothelium: Regulation of Endothelial Permeability, in: Moncada, S., Higgs, A. (Eds.), The Vascular Endothelium I. Springer Berlin Heidelberg, Berlin, Heidelberg, pp. 107–144. https://doi.org/10.1007/3-540-32967-6_4

Moore, T.A., Brodersen, P., Young, E.W.K., 2017. Multiple Myeloma Cell Drug Responses Differ in Thermoplastic vs PDMS Microfluidic Devices. Anal. Chem. 89, 11391–11398. https://doi.org/10.1021/acs.analchem.7b02351

Polacheck, W.J., Kutys, M.L., Tefft, J.B., Chen, C.S., 2019. Microfabricated blood vessels for modeling the vascular transport barrier, Nature Protocols. Springer US. https://doi.org/10.1038/s41596-019-0144-8

Rabiet, M.J., Plantier, J.L., Rival, Y., Genoux, Y., Lampugnani, M.G., Dejana, E., 1996. Thrombin-induced increase in endothelial permeability is associated with changes in cell-to-cell junction organization. Arterioscler. Thromb. Vasc. Biol. 16, 488–496. https://doi.org/10.1161/01.ATV.16.3.488

Ramanujan, S., Pluen, A., McKee, T.D., Brown, E.B., Boucher, Y., Jain, R.K., 2002. Diffusion and Convection in Collagen Gels: Implications for Transport in the Tumor Interstitium. Biophys. J. 83, 1650–1660. https://doi.org/10.1016/S0006-3495(02)73933-7

Sakolish, C.M., Esch, M.B., Hickman, J.J., Shuler, M.L., Mahler, G.J., 2016. Modeling Barrier Tissues In Vitro: Methods, Achievements, and Challenges. EBioMedicine 5, 30–39. https://doi.org/10.1016/j.ebiom.2016.02.023

Srinivasan, B., Kolli, A.R., Esch, M.B., Abaci, H.E., Shuler, M.L., Hickman, J.J., 2015. TEER Measurement Techniques for In Vitro Barrier Model Systems. J. Lab. Autom. 20, 107–126. https://doi.org/10.1177/2211068214561025

Trietsch, S.J., Naumovska, E., Kurek, D., Setyawati, M.C., Vormann, M.K., Wilschut, K.J., Lanz, H.L., Nicolas, A., Ng, C.P., Joore, J., Kustermann, S., Roth, A., Hankemeier, T., Moisan, A., Vulto, P.,

2017. Membrane-free culture and real-time barrier integrity assessment of perfused intestinal epithelium tubes. Nat. Commun. 8, 262. https://doi.org/10.1038/s41467-017-00259-3

Tung, C.K., Krupa, O., Apaydin, E., Liou, J.J., Diaz-Santana, A., Kim, B.J., Wu, M., 2013. A contact line pinning based microfluidic platform for modelling physiological flows. Lab Chip 13, 3876–3885. https://doi.org/10.1039/c3lc50489a

van der Helm, M.W., Odijk, M., Frimat, J.-P., van der Meer, A.D., Eijkel, J.C.T., van den Berg, A., Segerink, L.I., 2016. Direct quantification of transendothelial electrical resistance in organs-on-chips. Biosens. Bioelectron. 85, 924–929. https://doi.org/10.1016/j.bios.2016.06.014

van Duinen, V., van den Heuvel, A., Trietsch, S.J., Lanz, H.L., van Gils, J.M., van Zonneveld, A.J., Vulto, P., Hankemeier, T., 2017. 96 perfusable blood vessels to study vascular permeability in vitro. Sci. Rep. 7, 18071. https://doi.org/10.1038/s41598-017-14716-y

Vestweber, D., 2008. VE-Cadherin. Arterioscler. Thromb. Vasc. Biol. 28, 223–232. https://doi.org/10.1161/ATVBAHA.107.158014

Vulto, P., Glade, N., Altomare, L., Bablet, J., Del Tin, L., Medoro, G., Chartier, I., Manaresi, N., Tartagni, M., Guerrieri, R., 2005. Microfluidic channel fabrication in dry film resist for production and prototyping of hybrid chips. Lab Chip 5, 158–162. https://doi.org/10.1039/b411885e

Vulto, P., Medoro, G., Altomare, L., Urban, G.A., Tartagni, M., Guerrieri, R., Manaresi, N., 2006. Selective sample recovery of DEP-separated cells and particles by phaseguide-controlled laminar flow. J. Micromechanics Microengineering 16, 1847–1853. https://doi.org/10.1088/0960-1317/16/9/013

Wong, J.F., Simmons, C.A., 2019. Microfluidic assay for the on-chip electrochemical measurement of cell monolayer permeability. Lab Chip 19, 1060–1070. https://doi.org/10.1039/C8LC01321G

Wong, J.F., Simmons, C.A., Young, E.W.K., 2017a. Modeling and Measurement of Biomolecular Transport and Sensing in Microfluidic Cell Culture and Analysis Systems, in: Modeling of Microscale Transport in Biological Processes. Elsevier, pp. 41–75. https://doi.org/10.1016/B978-0-12-804595-4.00003-1

Wong, J.F., Young, E.W.K., Simmons, C.A., 2017b. Computational analysis of integrated biosensing and shear flow in a microfluidic vascular model. AIP Adv. 7, 115116. https://doi.org/10.1063/1.5006655

Yen, D.P., Ando, Y., Shen, K., 2016. A cost-effective micromilling platform for rapid prototyping of microdevices. Technology 04, 234–239. https://doi.org/10.1142/s2339547816200041

Yeste, J., Illa, X., Alvarez, M., Villa, R., 2018. Engineering and monitoring cellular barrier models. J. Biol. Eng. 12, 1–19. https://doi.org/10.1186/s13036-018-0108-5

Yuan, S.Y., Rigor, R.R., 2011. Regulation of Endothelial Barrier Function. Colloq. Ser. Integr. Syst. Physiol. From Mol. to Funct. 3, 1–146. https://doi.org/10.4199/C00025ED1V01Y201101ISP013

Zervantonakis, I.K., Hughes-Alford, S.K., Charest, J.L., Condeelis, J.S., Gertler, F.B., Kamm, R.D., 2012. Three-dimensional microfluidic model for tumor cell intravasation and endothelial barrier function. Proc. Natl. Acad. Sci. 109, 13515–13520. https://doi.org/10.1073/pnas.1210182109

- An electrochemical endothelial permeability assay was developed
- Unlike the standard fluorescent assay, an electroactive tracer was used
- The electrochemical format eliminated the need for complex, bulky optical instrumentation
- The method was shown to operate in a 3D cell culture environment

Conflict of Interest statement

The authors declare that they have no known competing financial interests or personal relationships that could have appeared to influence the work reported in this paper.

Declaration of interests

☒ The authors declare that they have no known competing financial interests or personal relationships that could have appeared to influence the work reported in this paper.

☐The authors declare the following financial interests/personal relationships which may be considered as potential competing interests: